Chemical Engineering Journal 145 (2009) 399–411

Contents lists available at ScienceDirect

Chemical Engineering Journal

journal homepage: www.elsevier.com/locate/cej

Linear stability analysis of high- and low-dimensional models for describing mixing-limited pattern formation in homogeneous autocatalytic reactors

Ankur Gupta, Saikat Chakraborty*

Department of Chemical Engineering, Indian Institute of Technology – Kharagpur, Kharagpur 721302, India

ARTICLE INFO

Article history:
Received 9 April 2008
Received in revised form 24 August 2008
Accepted 25 August 2008

Keywords:
Mixing
Pattern formation
Spatial averaging
Liapunov–Schmidt (L–S) technique
Homogeneous reaction
Autocatalytic reaction

ABSTRACT

In this paper, we perform linear stability analysis of high- and low-dimensional models for describing mixing-limited pattern formation in fast, homogeneous autocatalytic reactions occurring in isothermal tubular reactors. We consider three different models of varying dimensionality—the 3D convection-diffusion-reaction (CDR) model is the high dimensional one, and the Liapunov–Schmidt reduction based spatially averaged two-dimensional CDR model and its regularized form are the two low-dimensional ones. For each of these three models, steady state bifurcation diagrams that show the presence of multiple steady states were obtained and the stability of these multiple steady states to transverse perturbations was analyzed using linear stability analysis. Parametric analysis of the steady state bifurcation diagrams shows that for sufficiently large values of transverse Péclet number p, mixing-limited patterns may emerge from the unstable middle branch that connects the ignition and extinction points of an S-shaped bifurcation curve. Comparison of the bifurcation diagrams and the stability boundaries of the two low-dimensional models with that of the 3D CDR model reveals that the regularized form of the low-dimensional model has higher accuracy and a larger region of validity than the averaged form and is therefore recommended over the latter.

1. Introduction

It is well known that strong coupling between transport and reaction rate processes in chemical reactors gives rise to a variety of spatio-temporal patterns resulting from multiple steady states. Spatial pattern formation was first studied by Turing [1] in 1952. Later Nicolis and Prigogine [2] suggested a mechanism of symmetry-breaking and pattern formation in non-equilibrium systems, with Prigogine and coworkers developing the Brusselator model [3–5] that exhibits Turing instability. Transport-limited patterns are generated in autocatalytic reaction systems when a spatially uniform steady state loses its stability to transverse perturbations, and the patterns, once formed, are sustained when local mixing/diffusion is slower as compared to reaction. Localized hot zone formation is one such example where an asymmetrical temperature profile exists in the reactor cross-section.

Temperature patterns were observed in packed bed reactors during partial oxidation of isobutyl alcohol by Boreskov et al. [6] and Matros [7], in trickle bed reactors by Barkelew and Gambhir [8], and in radial flow and packed bed reactors by Luss and coworkers [9,10]. Such a condition can often decrease the yield of the desired product, deactivate the catalyst, initiate highly exothermic undesirable reactions or induce safety hazards by decreasing the reactor strength.

Most modeling attempts in the literature aimed at predicting pattern formation have been focused on heterogeneous packed bed and catalytic reactors. Early theoretical studies by Luss et al. [11] investigated the existence of asymmetric steady states in catalytic slabs using one-dimensional diffusion-reaction models. Schmitz and Tsotsis [12] showed in their theoretical study that inter-particle interactions give rise to spatially patterned states under certain conditions. Balakotaiah and coworkers [13–15] have shown that flow misdistributions and hot spots may occur in down-flow packed-bed reactors and the regions of these instabilities are determined in terms of various transport and kinetic parameters. Benneker et al. [16] indicated that hydrodynamic instabilities observed in packed-bed reactors may disturb the plug-flow character and may lead to hot spots and deactivated catalysts. Balakotaiah and coworkers predicted transverse pattern formation in adiabatic packed bed reactors in which a bimolecular reaction (with Langmuir–Hinshelwood kinetics) occurs [17], and in catalytic monolith reactors in which an exothermic surface reaction occurs [18]. Sheintuch and Nekhamkina [19] analyzed the pattern formation in homogeneous model of a fixed catalytic bed for reactions with oscillatory kinetics. Viswanathan and Luss [20–22] have stud-

* Corresponding author. Tel.: +91 32222 83930; fax: +91 32222 82250.
E-mail address: Dr.S.Chakraborty@gmail.com (S. Chakraborty).

1385-8947/$ – see front matter © 2008 Elsevier B.V. All rights reserved.
doi:10.1016/j.cej.2008.08.025

Nomenclature

a	radius of the tubular reactor
a_i	coefficients of terms in the expansion of polynomial P
a_{ij}	terms of matrix A
A	matrix of coefficients for the system of equations after discretization
b_i	coefficients of terms in the expansion of polynomial Q
B	vector of coefficients for the system of equations after discretization
c	dimensionless reactant concentration
c_0	initial dimensionless reactant concentration
$\bar{c}$	axially averaged dimensionless reactant concentration
c_e	dimensionless exit concentration
c_{ss}	steady state dimensionless concentration
c_ν	dimensionless perturbation concentration term
c_i	coefficients of terms in the expansion of polynomial R
C	reactant concentration
C_{in}	inlet concentration
C_0	initial concentration in the reactor
Da	Damköhler number
D_c	Fréchet derivative
D_m	molecular diffusivity
$D_{A(B)}$	diffusivity of species $A(B)$
f	eigenfunction in axial direction
F	non-linear operator
J_m	Bessel function of the first kind
k	reaction rate constant
k_{mn}	wave number
L	length of the tubular reactor
L_e	effective reactor length
m	azimuthal mode numbers
n	radial mode numbers
N	number of points used in discretization plus one
p	transverse Péclet number
Pe	axial Péclet number
r	dimensionless reaction rate
$R_{A(B)}$	rate of disappearance of $A(B)$
t	dimensionless time
t'	time
t_d	characteristic radial diffusion time
t_Z	characteristic axial diffusion time
t_R	characteristic reaction time
$\boldsymbol{u}$	velocity field
u_x	dimensionless axial velocity
u'_x	axial velocity
$\bar{u}'_x$	averaged axial velocity
W	transverse slave modes
x	axial coordinate
$X_{A(B)}$	conversion of species $A(B)$
z	dimensionless axial time

Greek letters

α	coefficients of the neutral stability relation for 3D model
β	parameter defined as ratio of Damkohler number to axial Péclet number
γ	coefficient of terms in the expansion of $\bar{c} - c_e$
η	parameter in power series expansion of polynomials P, Q, R
θ	azimuthal coordinate
λ	coefficient of time in the exponential term
μ	inlet feeding ratio of B to A
μ_0	eigenvalue corresponding to the master mode
ξ	dimensionless radial coordinate
ξ'	radial coordinate
τ_C	characteristic convection time
ψ_0	eigenfunction corresponding to the master mode
L	linear operator

ied the conditions for the existence of hot zones in a uniformly active shallow as well as long adiabatic packed bed reactors using a two-phase model.

Mathematical models developed to study chemical reactors are derived from balances of species, energy, momentum and continuity in conjunction with various constitutive relationships, and they form a set of unsteady state three-dimensional partial differential equations containing a large set of physiochemical parameters. The detailed model is rendered even more complex due to the non-linear dependence of kinetic and transport coefficients on the state variables. The bottom-up approach of using computational fluid dynamics (CFD) to explore the solutions of the three-dimensional convection-diffusion-reaction (CDR) equation in the multi-dimensional parameter space is numerically very expensive, and is fairly impractical even with present day computational technology, especially when incorporating the model to existing control strategies. Even in cases where exact numerical solutions are possible, further averaging or coarse-graining is required to obtain results suitable for engineering purposes. On the other hand, the top-down approach – which is to make *a priori* oversimplifying assumptions on the length and time scales of reaction, convection and diffusion and then apply conservation equations only at the macroscopic levels – though easy to solve, are incapable of capturing the complex spatio-temporal reactor behaviors such as multiplicity, pattern/hot-zone formation, and reactor runaway that are observed during operation. Accurate low-dimensional models that are numerically inexpensive yet retain all the qualitative features of the 3D CDR model are required for the purpose of design, control and optimization of a chemical process. Such an intermediate approach has been presented by Chakraborty and Balakotaiah [23–26], in which the fundamental three-dimensional CDR equation is averaged or homogenized over the smaller length (time) scales using Liapunov–Schimdt (L–S) technique [27] of the classical bifurcation theory to obtain low-dimensional models that retain all the parameters and therefore all the spatio-temporal features of the full CDR equation. The reduced dimensionality of the models substantially reduces the computational expense required, thus making it suitable for engineering applications.

In this paper, we consider the case of an isothermal tubular reactor with homogeneous autocatalytic reaction kinetics. It has been shown previously for this case [28] that patterned states are generated when the characteristic mixing time of the system is larger than the reaction time. Considering the case of very fast reactions (i.e., diffusion/local mixing time $\gg$ reaction time) such that scale separation exists between the characteristic reaction and local mixing time scales, we homogenize the three-dimensional CDR equation using the L–S technique along the short axial length over which the reaction is complete. The reduced model is a two-dimensional two-mode model that retains all the parameters of the CDR equation, which is then used to analyze pattern formation

in the reactor with autocatalytic reaction of the type $A+2B\rightarrow 3B$. Further, we extend the region of validity of this axially averaged two-mode model by using a mathematical procedure called regularization to obtain a *regularized model*, which is then subjected to the same treatment. For each of these three models (the 3D CDR and its averaged and regularized forms), steady state bifurcation diagrams are obtained, which show the presence of multiple steady states, and the stability of these multiple solutions to transverse perturbations is examined using linear stability analysis. *Analytical expressions* describing steady state solutions and neutral stability conditions are obtained for the case of low-dimensional models, which are very difficult to obtain for the 3D model. The effects of various parameters on the nature and location of stability boundaries are also determined.

A dynamic simulation of patterned states using the averaged and regularized low-dimensional models for the isothermal [29] and the non-isothermal cases [30] show that the temporal evolution of patterned states from a homogeneous, unstable steady state is characterized by a process of concentration-segregation followed by a gradual decay of non-homogeneity with eventual return to a homogeneous stable steady state at time scales much larger than reactor residence time. Patterned states have been simulated in [29] and [30] by solving the non-linear unsteady state CDR equations for the averaged and regularized models. The homogeneous unstable steady state is perturbed using three kinds of perturbation (namely, band, antiphase and target), and the resulting evolution of patterned states is studied along with the effects of various parameters on such an evolution.

2. Mathematical modeling

2.1. Three-dimensional model

We consider the case of a tubular reactor of uniform cross-section with length L and hydraulic radius a, in which a homogeneous autocatalytic reaction given by

$$A+2B\xrightarrow{k}3B, \tag{1}$$

occurs. The rates of disappearance of A and B are given by

$$R_A=-R_B=kC_AC_B^2. \tag{2}$$

The scalar concentration $C(x,\xi',\theta,t')$ of any species obeys the CDR equation given by

$$\frac{\partial C}{\partial t}+\boldsymbol{u}\cdot\nabla C=\nabla\cdot(D_{\mathrm{m}}\nabla C)-R(C), \tag{3}$$

where $\boldsymbol{u}(x,\xi',\theta,t')$ is the velocity field, D_{m} is the molecular diffusivity, and $R(C)$ is the volumetric sink term due to homogeneous chemical reaction, with flux-type (Robin) boundary condition at the entrance and no-flux type (Neumann) boundary condition on all other surfaces. The symbols x,ξ',θ and t' represent the three spatial coordinates (axial, radial and azimuthal) and time, respectively. When the velocity profile is unidirectional (in axial direction), Eq. (3) is simplified for species A and B, respectively, to

$$\frac{\partial C_i}{\partial t'}+u_x'\frac{\partial C_i}{\partial x}=D_i\frac{\partial^2 C_i}{\partial x^2}+D_i\left[\frac{1}{\xi'}\frac{\partial}{\partial\xi'}\left(\xi'\frac{\partial C_i}{\partial\xi'}\right)+\frac{1}{\xi'^2}\frac{\partial^2 C_i}{\partial\theta^2}\right]-R_i,\quad (i=A,B), \tag{4}$$

where R_i (for $i=A,B$) is given by Eq. (2). The boundary conditions (for $i=A,B$) are given by

$$\text{at } x=0,\quad D_i\frac{\partial C_i}{\partial x}=u_x'(C_i-C_{i,\mathrm{in}}), \tag{5}$$

$$\text{at } x=L,\quad \frac{\partial C_i}{\partial x}=0, \tag{6}$$

$$\text{at } \xi'=0,\quad C_i \text{ is finite}, \tag{7}$$

$$\text{at } \xi'=a,\quad \frac{\partial C_i}{\partial\xi'}=0, \tag{8}$$

$$C_i(x,\xi',\theta,t')=C_i(x,\xi',\theta+2\pi,t'), \tag{9}$$

and the initial condition (for $i=A,B$) is given by

$$\text{at } t'=0,\quad C_i(x,\xi',\theta,0)=C_{i0}(x,\xi',\theta). \tag{10}$$

Taking L and a as characteristic length scales in axial and radial directions, respectively, C_{R} as the reference concentration and $\bar{u}'_x$ as the average velocity, we obtain four time scales in the system, associated with convection (τ_{C}), radial diffusion (t_{d}), axial diffusion (t_Z) and reaction (t_{R}), which are given as

$$\tau_{\mathrm{C}}=\frac{L}{\bar{u}'_x},\quad t_{\mathrm{d}}=\frac{a^2}{D_{\mathrm{m}}},\quad t_z=\frac{L^2}{D_{\mathrm{m}}},\quad t_{\mathrm{R}}=\frac{C_{\mathrm{R}}}{R(C_{\mathrm{R}})}, \tag{11}$$

respectively. Using these time scales we obtain three independent dimensionless numbers: transverse Péclet number (p), axial Péclet number (Pe), and Damköhler number (Da), which are given as

$$p=\frac{t_{\mathrm{d}}}{\tau_{\mathrm{C}}}=\frac{a^2\bar{u}'_x}{LD_{\mathrm{m}}},\quad Pe=\frac{t_Z}{\tau_{\mathrm{C}}}=\frac{\bar{u}'_xL}{D_{\mathrm{m}}},\quad Da=\frac{\tau_{\mathrm{C}}}{t_{\mathrm{R}}}=\frac{LR(C_{\mathrm{R}})}{\bar{u}'_xC_{\mathrm{R}}}, \tag{12}$$

respectively. Another parameter can be defined as the ratio of Damköhler number to axial Péclet number, given by

$$\beta=\frac{Da}{Pe}=\frac{D_{\mathrm{m}}R(C_{\mathrm{R}})}{\bar{u}'_{x^2}C_{\mathrm{R}}}=\frac{\tau_{\mathrm{C}}^2}{t_{\mathrm{R}}t_Z}. \tag{13}$$

Thus, β involves all the timescales in the system, excluding the one in the transverse direction (i.e., t_{d}), and is independent of the radial and axial dimensions of the reactor.

In this work, we study the formation of patterned states as a result of difference in transverse mixing rates and reaction rates and not due to difference of molecular diffusivities of different species. Therefore, diffusivities of both species A and B are taken to be equal, i.e., $D_{\mathrm{m}}=D_A=D_B$.

The three-dimensional CDR equation given in Eq. (4) is made dimensionless by using the following dimensionless variables and parameters

$$c=\frac{C}{C_{\mathrm{R}}},\quad \xi=\frac{\xi'}{a},\quad z=\frac{x}{L},\quad t=\frac{t}{\tau_{\mathrm{C}}},\quad r(c)=\frac{R(C)}{R(C_{\mathrm{R}})},\quad u_x=\frac{u'_x}{\bar{u}'_x}. \tag{14}$$

Assuming a flat velocity profile such that $u_x=1$ and taking $C_{\mathrm{R}}=C_{A,\mathrm{in}}$, the 3D CDR equations for species A and B in the dimensionless form are given by (for $i=A,B$),

$$\frac{\partial c_i}{\partial t}+\frac{\partial c_i}{\partial z}+Da\,r_i=\frac{\beta}{Da}\frac{\partial^2 c_i}{\partial z^2}+\frac{1}{p}\left[\frac{1}{\xi}\frac{\partial}{\partial\xi}\left(\xi\frac{\partial c_i}{\partial\xi}\right)+\frac{1}{\xi^2}\frac{\partial^2 c_i}{\partial\theta^2}\right], \tag{15}$$

respectively, where, $r_A=-r_B=c_Ac_B^2$. Similarly, the boundary conditions (for $i=A,B$) can be written in dimensionless form as

$$\text{at } z=0,\quad \frac{\beta}{Da}\frac{\partial c_i}{\partial z}-c_i+\mu_i=0, \tag{16}$$

where $\mu_A=1$, $\mu_B=C_{B,\mathrm{in}}/C_{A,\mathrm{in}}=\mu$,

$$\text{at } z=1,\quad \frac{\partial C_i}{\partial z}=0, \tag{17}$$

$$\text{at } \xi=0,\quad c_i \text{ is finite}, \tag{18}$$

$$\text{at } \xi=1,\quad \frac{\partial C_i}{\partial\xi}=0, \tag{19}$$

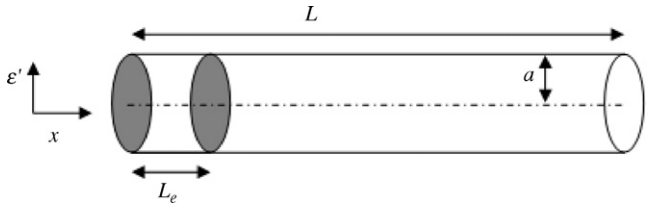

Fig. 1. Schematic diagram of a tubular reactor, showing the effective reactor length (L_e), and the length scales in transverse (a) and axial (L) directions.

$$c_i(z, \xi, \theta, t) = c_i(z, \xi, \theta + 2\pi, t), \tag{20}$$

The initial condition (for $i = A, B$) are given by

$$\text{at } t = 0, \quad c_i(z, \xi, \theta, 0) = c_{i0}(z, \xi, \theta). \tag{21}$$

2.2. Liapunov–Schmidt reduction-based averaging of the 3D CDR model

We have considered the case of a very fast reaction such that a separation of time/length scales (between transverse diffusion and reaction) exists in the system. The reaction is completed within a small axial length of the reactor, which is called the effective reactor length, L_e, and is given by [28]

$$\frac{L_e}{a} \sim \sqrt{\frac{t_R}{\beta_1 t_d}}. \tag{22}$$

Fig. 1 shows a schematic diagram of a tubular reactor with the effective reactor length L_e. It is obvious that for the case of a fast reaction, $t_R \ll t_d$, as a result of which $L_e \ll a$. Therefore, $L_e \ll L$, since typically $a < L$. Nevertheless, neglecting the length L_e would be an oversimplifying assumption resulting in loss of one parameter—the axial Péclet number, Pe. Instead, we homogenize the CDR equation over the short axial length, L_e, using Liapunov–Schimdt technique [23] to obtain a low-dimensional model that – unlike traditional oversimplified models developed using the top–down approach – retains all the parameters of the original CDR equation. Consequently, our low-dimensional models are capable of capturing complex spatio-temporal patterns that are often missed by the traditional low-dimensional models [29,30]. Further, this low-dimensional model obtained after L–S averaging, unlike traditional models, is described by two concentration variables instead of one; hence the name *two-mode model* [24].

Details of transverse averaging of a homogeneous tubular reactor can be found in [23]. Axial averaging of a homogeneous tubular reactor using the same technique can be found in [28]. In this paper, for the sake of brevity, we do not present the complete derivation of the axially averaged model using Liapunov–Schmidt averaging, and instead, we summarize the main steps involved in the rigorous averaging of the three-dimensional CDR model.

The three-dimensional CDR equation which is applicable for both species A and B can be written in dimensionless form (in terms of the parameters p, Pe and Da) as

$$\frac{\partial c}{\partial t} + u_x(\xi)\frac{\partial c}{\partial z} + Da\ r(c) = \frac{1}{Pe}\frac{\partial^2 c}{\partial z^2} + \frac{1}{p}\left[\frac{1}{\xi}\frac{\partial}{\partial \xi}\left(\xi\frac{\partial c}{\partial \xi}\right) + \frac{1}{\xi^2}\frac{\partial^2 c}{\partial \theta^2}\right]. \tag{23}$$

We consider the non-linear function

$$F(c, Pe) \equiv \frac{\partial^2 c}{\partial z^2} - Pe\left[\frac{\partial c}{\partial t} + u_x(\xi)\frac{\partial c}{\partial z} - Da\ r(c) - \frac{1}{p}\left\{\frac{1}{\xi}\frac{\partial}{\partial \xi}\left(\xi\frac{\partial c}{\partial \xi}\right) + \frac{1}{\xi^2}\frac{\partial^2 c}{\partial \theta^2}\right\}\right] = 0, \tag{24}$$

with the boundary conditions being given by

$$\text{at } z = 0, \quad \frac{1}{Pe}\frac{\partial c}{\partial z} - c + \mu_i = 0, \tag{25}$$

$$\text{at } z = 1, \quad \frac{\partial c}{\partial z} = 0, \tag{26}$$

$$\text{at } \xi = 0, \quad c \text{ is finite}, \tag{27}$$

$$\text{at } \xi = 1, \quad \frac{\partial c}{\partial \xi} = 0, \tag{28}$$

$$c(z, \xi, \theta, t) = c(z, \xi, \theta + 2\pi, t). \tag{29}$$

For the base state, i.e. $Pe = 0$ (or in other words, when axial mixing is complete down to the molecular level), the solution to Eq. (24) is $c = \bar{c}$ and

$$\mathcal{L}v = D_c F(\bar{c}, 0)v = \frac{d^2 v}{dz^2} = 0, \tag{30}$$

with $dc/dz = 0$ at $z = 0, 1$, where L is a linear operator operating on a variable v, and $D_c F(\bar{c}, 0)$ is the first-order Fréchet derivative of the function F (defined in Eq. (24)), evaluated at $c = \bar{c}$, $Pe = 0$. Here $\dim(\ker L) = 1$; L has a zero eigenvalue ($\mu_0 = 0$) and corresponding eigenfunction is $\psi_0 = 1$ ($\psi_0 \in \ker L$) normalized with respect to the inner product

$$\langle u, v \rangle = \int_0^1 uv\, dz. \tag{31}$$

Here, ψ_0 represents the leading master mode, which in this case is a mode without axial variation and W represents the slave modes with axial variation but zero axial average. Therefore, $W \perp \ker L$, or in other words, $\langle W, \psi_0 \rangle = 0$, (where the inner product is defined by Eq. (31)), and we can write $c(z, \xi, \theta, t)$ as

$$c(z, \xi, \theta, t) = \langle c, \psi_0 \rangle \psi_0 + W = \bar{c}(\xi, \theta, t) + W(z, \xi, \theta, t). \tag{32}$$

L is self-adjoint (i.e., $L^* =$ adjoint operator $= L$) and the projection onto the range L is defined by $EF = F - \langle F, \psi_0 \rangle \psi_0$, and the projection onto the ker L^* is defined by $(I - E)F = \langle F, \psi_0 \rangle \psi_0$. If $F = 0$, then the projections of F onto these two orthogonal planes have to be zero, i.e.,

$$F(\bar{c} + W, Pe) - \int_0^1 F(\bar{c} + W, Pe)\, dz = 0, \tag{33}$$

$$\int_0^1 F(\bar{c} + W, Pe)\, dz = 0. \tag{34}$$

Eq. (34) is called the branching equation, which has to be solved in conjunction with Eq. (33) in order to obtain the transverse slave modes $W(z, \xi, \theta, t)$. For the case of fast reactions, the perturbation parameter Pe is defined in terms of effective reactor length L_e (instead of the actual length L) and is obtained on the basis of the assumption that the time scales of axial diffusion based on L_e ($t_Z = L_e^2/D_m$) and reaction ($t_R = C_R/R(C_R)$) are of the same order of magnitude [28]. Thus, Pe (in Eq. (12)) is given by

$$Pe = \frac{\bar{u}'_x L_e}{D_m} = \sqrt{\frac{\bar{u}'^2_x C_R}{D_m R(C_R)}}. \tag{35}$$

As is evident, Pe is a small parameter in case of fast reactions, and, therefore, we carry out an expansion of W in terms of Pe as

$$\begin{aligned} W &= Pe\ W_1 + Pe^2 W_2 + Pe^3 W_3 + \text{h.o.t.}, \\ r(\bar{c} + W) &= r(\bar{c}) + Pe\ W_1 r'(\bar{c}) + \text{h.o.t.} \end{aligned} \tag{36}$$

In order to obtain the low-dimensional equations by averaging over the effective length of the reactor, we require at least two independent modes, the difference of which quantifies the amount of axial

mixing. In addition to the axially averaged concentration $\bar{c}$, which is the master mode and is defined as

$$\bar{c}(\xi,\theta,t) = \int_0^1 c(z,\xi,\theta,t)\ \mathrm{d}z, \tag{37}$$

we define another mode c_e (exit concentration) as

$$c_e(\xi,\theta,t) = c(z=1,\xi,\theta,t). \tag{38}$$

Using these two modes and the expansion of W in terms of Pe (Eq. (36)), we perform the Liapunov–Schmidt reduction-based spatial averaging of Eq. (24), with the boundary conditions given by Eqs. (25)–(29) to obtain the low-dimensional axially averaged model described by a pair of coupled differential-algebraic equations, known as global and local equations, respectively, and are presented below.

Global equation:

$$p\left[\frac{\partial\bar{c}}{\partial t} + u_x(\xi)[c_e - c_{in}] + Da\, r(\bar{c})\right] = \frac{1}{\xi}\frac{\partial}{\partial\xi}\left(\xi\frac{\partial\bar{c}}{\partial\xi}\right) + \frac{1}{\xi^2}\frac{\partial^2\bar{c}}{\partial\theta^2}, \tag{39}$$

Local equation:

$$\bar{c} - c_e = \frac{Pe}{6}u_x(\xi)[c_{in} - c_e], \tag{40}$$

where the two modes $\bar{c}$ and c_e are given by Eqs. (37) and (38), respectively. Here, $\bar{c}$ is the axially averaged concentration in the reactor and c_e is the concentration at the reactor exit. It may be noted that all the three parameters of the original 3D CDR equation are retained between the global and local equations. The axial Péclet number (Pe) in Eq. (40) is based on the effective reactor length L_e (as given by Eq. (22)). The boundary conditions for Eqs. (39) and (40) are given by

$$\text{at } \xi = 0, \quad \bar{c} \text{ is finite}, \tag{41}$$

$$\text{at } \xi = 1, \quad \frac{\partial\bar{c}}{\partial\xi} = 0, \tag{42}$$

$$\bar{c}(\xi,\theta,t) = \bar{c}(\xi,\theta+2\pi,t). \tag{43}$$

The initial condition is given as

$$\text{at } t = 0, \quad \bar{c}(\xi,\theta,0) = \bar{c}(\xi,\theta). \tag{44}$$

The region of validity for this model could be obtained in terms of the parameters by considering higher order terms (of Pe) in the series given in Eq. (36) and examining the radius of convergence of the local equation, as had been done by Chakraborty and Balakotaiah [23] for the case of transverse averaging of a tubular reactor. The same may be done for axial averaging of a tubular reactor; derivation of which is beyond the purview of this work. However a detailed derivation could be found in [28]. Inspection of the axially averaged model reveals that the model is not valid for conditions of $Pe \geq 6$. However, the actual radius of convergence of the local equation corresponds to a value of Pe smaller than 6. Rearranging Eq. (40), we get

$$c_e - c_{in} = \frac{\bar{c} - c_{in}}{1 - (Pe/6)u_x(\xi)}. \tag{45}$$

Using Eqs. (39) and (45), Eqs. (39) and (40) could be rewritten in a single equation form in terms of $\bar{c}$ as

$$p\left[\frac{\partial\bar{c}}{\partial t} + u_x(\xi)\frac{\bar{c} - c_{in}}{1 - (Pe/6)u_x(\xi)} + Da\ r(\bar{c})\right] = \frac{1}{\xi}\frac{\partial}{\partial\xi}\left(\xi\frac{\partial\bar{c}}{\partial\xi}\right) + \frac{1}{\xi^2}\frac{\partial^2\bar{c}}{\partial\theta^2}, \tag{46}$$

Writing Eq. (46) for $i = A, B$, for a flat velocity profile, we simplify the model equation to

$$p\left[\frac{\partial\bar{c}_i}{\partial t} + \frac{\bar{c}_i - c_{i,in}}{1 - (Da/6\beta)} + Da\, r_i(\bar{c})\right] = \frac{1}{\xi}\frac{\partial}{\partial\xi}\left(\xi\frac{\partial\bar{c}_i}{\partial\xi}\right) + \frac{1}{\xi^2}\frac{\partial\bar{c}_i}{\partial\theta^2}, \tag{47}$$

where, $r_A(\bar{c}) = -r_B(\bar{c}) = \bar{c}_A\bar{c}_B^2$. The boundary conditions (for $i = A, B$) are given by

$$\text{at } \xi = 0, \quad \bar{c}_i \text{ is finite}, \tag{48}$$

$$\text{at } \xi = 1, \quad \frac{\partial\bar{c}_i}{\partial\xi} = 0, \tag{49}$$

$$\bar{c}_i(\xi,\theta,t) = \bar{c}_i(\xi,\theta+2\pi,t), \tag{50}$$

The initial conditions (for $i = A, B$) are given as

$$\text{at } t = 0, \quad \bar{c}_i(\xi,\theta,0) = \bar{c}_{i0}(\xi,\theta). \tag{51}$$

The parameter β is given by Eq. (13). We will refer to this model (described by Eqs. (47)–(51)) as the *averaged model*.

2.3. Regularization of axially averaged model

As mentioned in the previous section, the radius of convergence of the local equation is given by $Pe < 6$. Outside the region of convergence, the averaged models are quantitatively (and sometimes even qualitatively) inaccurate. Here, we utilize the mathematical technique of *regularization* to increase the radius of convergence of the equation, which in turn would increase the region of validity of the low-dimensional models.

Consider a function defined by an infinite power series in terms of a parameter η, given by

$$R = c_0 + c_1\eta + c_2\eta^2 + c_3\eta^3 + \cdots \tag{52}$$

Usually, one truncates the series retaining terms till a particular order; however, outside the region of convergence of the series, inclusion of higher order terms does not make the series convergent. Thus, in cases where the power series is poorly convergent or even non-convergent, we can use Padé's approximation to rectify this problem and increase the region of convergence and validity of the series. Unlike the power series that expresses the function in terms of a single polynomial, Padé's approximation represents the function as a ratio of two polynomials

$$R = \frac{P}{Q}, \tag{53}$$

where

$$\begin{aligned} P &= a_0 + a_1\eta + a_2\eta^2 + a_3\eta^3 + \cdots \\ Q &= 1 + b_1\eta + b_2\eta^2 + b_3\eta^3 + \cdots + b_n\eta^n \end{aligned} \tag{54}$$

The central idea in regularization is to make a suitable choice of the polynomial Q so as to increase the radius of convergence of the original power series. In most cases, Padé's approximation provides a better approximation as compared to the original power series especially when $|\eta|$ is comparable to (or even greater than) the radius of convergence of the power series R [31].

In our case, the local equation obtained after Liapunov–Schmidt reduction is such a power series in terms of the perturbation parameter, Pe, of the form

$$\bar{c} - c_e = \gamma_1 Pe + \gamma_2 Pe^2 + \gamma_3 Pe^3 + \cdots \tag{55}$$

Instead of truncating the series to O(Pe) (as in the case of Eq. (40)), we employ the regularization technique [31] discussed above to obtain the *regularized model*, which is described by the following

equation:

$$p\left[\frac{\partial \bar{c}_i}{\partial t}+(\bar{c}_i-c_{i,\mathrm{in}})\left(1+\frac{Da}{6\beta}\right)+Da\, r_i(\bar{c})\right]=\frac{1}{\xi}\frac{\partial}{\partial \xi}\left(\xi\frac{\partial \bar{c}_i}{\partial \xi}\right)+\frac{1}{\xi^2}\frac{\partial \bar{c}_i}{\partial \theta^2}, \tag{56}$$

with the boundary and initial conditions being given by Eqs. (48)–(51). It may be observed that Eq. (56) is similar to Eq. (47), except for the coefficient of the $(\bar{c}_i - c_{i,\mathrm{in}})$ term ($i = A, B$). Thus, for the sake of brevity, the derivation of the steady state solution and neutral stability relation has been illustrated for the averaged model alone.

3. Steady state solutions and bifurcation diagrams

In this section, we obtain the homogeneous steady state solutions ($c_{A,\mathrm{ss}}$, $c_{B,\mathrm{ss}}$) to the three models obtained in Section 2. For the 3D model, we solve Eq. (15) for $c_{A,\mathrm{ss}}$ and $c_{B,\mathrm{ss}}$, which represent the steady state concentration of species A and B, respectively. It may be noted that for uniform feeding over the reactor cross-section, $c_{A,\mathrm{ss}}$ and $c_{B,\mathrm{ss}}$ are uniform and independent of the transverse coordinates. The same method is followed for Eqs. (47) and (56) to determine the steady state solutions of the averaged model and regularized model, respectively. Owing to the reduced (axial) dimensionality of the averaged and regularized models, their steady state solutions can be obtained by solving the cubic equations given by Eqs. (65) and (66), while that for the 3D model is given by a second-order ordinary differential equation.

3.1. Steady state solution of the three-dimensional CDR model

The one-dimensional steady state solution is obtained by solving the following simplified form of Eq. (15)

$$\frac{\mathrm{d}c_{i,\mathrm{ss}}}{\mathrm{d}z}+Da\, r_{i,\mathrm{ss}}=\frac{\beta}{Da}\frac{\mathrm{d}^2 c_{i,\mathrm{ss}}}{\mathrm{d}z^2}, \tag{57}$$

where $i = A$, B, and $r_{A,\mathrm{ss}} = -r_{B,\mathrm{ss}} = c_{A,\mathrm{ss}}c_{B,\mathrm{ss}}^2$. The boundary conditions are given by Eqs. (16) and (17). Taking the reference concentration $C_R = C_{A,\mathrm{in}}$, we get $C_{A,\mathrm{in}} = 1$ and $C_{B,\mathrm{in}} = \mu$. Adding Eqs. (57) for $i = A$ with that for $i = B$, we obtain

$$\frac{\mathrm{d}}{\mathrm{d}z}(c_{A,\mathrm{ss}}+c_{B,\mathrm{ss}})=\frac{\beta}{Da}\frac{\mathrm{d}^2}{\mathrm{d}z^2}(c_{A,\mathrm{ss}}+c_{B,\mathrm{ss}}). \tag{58}$$

Adding the boundary conditions given by Eqs. (16) and (17), we obtain

$$\text{at } z=0,\quad \frac{\beta}{Da}\frac{\partial}{\partial z}(c_{A,\mathrm{ss}}+c_{B,\mathrm{ss}})-(c_{A,\mathrm{ss}}+c_{B,\mathrm{ss}})+1+\mu=0, \tag{59}$$

$$\text{at } z=1,\quad \frac{\partial}{\partial z}(c_{A,\mathrm{ss}}+c_{B,\mathrm{ss}})=0, \tag{60}$$

Solving these equations for $(c_{A,\mathrm{ss}} + c_{B,\mathrm{ss}})$, we obtain the invariance

$$c_{A,\mathrm{ss}}+c_{B,\mathrm{ss}}=1+\mu, \tag{61}$$

substituting which in Eq. (57), we get

$$\frac{\mathrm{d}c_{A,\mathrm{ss}}}{\mathrm{d}z}+Da\, c_{A,\mathrm{ss}}(\mu+1-c_{A,\mathrm{ss}})^2=\frac{\beta}{Da}\frac{\mathrm{d}^2 c_{A,\mathrm{ss}}}{\mathrm{d}z^2}. \tag{62}$$

We solve Eq. (62) for $c_{A,ss}$ numerically by using second order finite difference method with reflection type boundary conditions. Eq. (61) is then used to find $c_{B,\mathrm{ss}}$. Arc length continuation technique is used to plot steady state bifurcation diagrams as exit conversion of species A versus Damköhler number Da.

3.2. Steady state solution of the averaged model

The steady state form of the averaged model is given by

$$p\left[\frac{\bar{c}_{i,\mathrm{ss}}-c_{i,\mathrm{in}}}{1-(Da/6\beta)}+\mathrm{Da}\, r_{i,\mathrm{ss}}(\bar{c})\right]=0, \tag{63}$$

where, $r_{A,\mathrm{ss}}(\bar{c}) = -r_{B,\mathrm{ss}}(\bar{c}) = \bar{c}_A\bar{c}_B^2$. Adding the above equations for $i = A$ and that for $i = B$, we obtain an invariance

$$\bar{c}_{A,\mathrm{ss}}+\bar{c}_{B,\mathrm{ss}}=1+\mu. \tag{64}$$

Substituting this relation in Eq. (63), we get the following relation, which is then used to find both $C_{A,\mathrm{ss}}$ and $C_{B,\mathrm{ss}}$, for a fixed value of parameters Da, β and μ

$$Da\left(1-\frac{Da}{6\beta}\right)\bar{c}_{B,\mathrm{ss}}^3-Da\left(1-\frac{Da}{6\beta}\right)(1+\mu)\bar{c}_{B,\mathrm{ss}}^2+\bar{c}_{B,\mathrm{ss}}-\mu=0. \tag{65}$$

This relation is then used to plot steady state bifurcation diagram of the exit steady state concentration of species A or B as a function of Da.

3.3. Steady state solution of the regularized model

We solve Eq. (56) in a manner similar to the one in Section 3.2 to obtain the steady state solution of the regularized model, which is given by

$$\left[\frac{Da}{(1+Da/6\beta)}\right]\bar{c}_{B,\mathrm{ss}}^3-\left[\frac{Da(1+\mu)}{(1+Da/6\beta)}\right]\bar{c}_{B,\mathrm{ss}}^2+\bar{c}_{B,\mathrm{ss}}-\mu=0. \tag{66}$$

It may be noted that Eq. (66) is similar in form to Eq. (65), and the invariance relation given by Eq. (64) holds good for the regularized model. Eqs. (64) and (66) are used to plot steady state bifurcation diagrams for the regularized model.

4. Linear stability analysis

In order to examine the stability of the steady state solutions (given by Eq. (62)) of the 3D CDR model to transverse perturbations, we write the state variables for $i = A$, B in the form

$$c_i = c_{i,\mathrm{ss}} + c_{iv} \tag{67}$$

where the perturbation terms, c_{iv} is of the form

$$c_{iv} = \mathrm{e}^{\lambda t} f_i(z) J_{\mathrm{m}}(\xi k_{mn})\mathrm{e}^{\mathrm{i}m\theta}, \tag{68}$$

where m and n are azimuthal and radial mode numbers, respectively, J_{m} is the Bessel function of the first kind, λ is the growth/decay coefficient and k_{mn} is the wave number that can be obtained by using the no flux boundary condition at $\xi = 1$, which is the nth nontrivial solution of the equation

$$\frac{\mathrm{d}}{\mathrm{d}\xi}J_{\mathrm{m}}(k_{mn}\xi)\Big|_{\xi=1}=mJ_{\mathrm{m}}(k_{mn})-k_{mn}J_{m+1}(k_{mn})=0. \tag{69}$$

Every value of k_{mn} corresponds to a mode of perturbation or eigen mode, e.g., $k_{11} = 1.8412$ corresponds to the first mode (shown in Fig. 2(a)). Regions indicated by 'H' represent high concentration of species i while 'L' represents regions of low concentration. All modes with $m = 0$ are azimuthally symmetric (as shown in Fig. 2(c)), while those with non-zero azimuthal mode number retain azimuthal variation.

It may be noted that, for the case of the two-dimensional models (averaged and regularized) the concentration is not a function of z and hence the variables c_i, $c_{i,\mathrm{ss}}$, c_{iv} will be replaced by their averaged counterparts, i.e., $\bar{c}_i$, $\bar{c}_{i,\mathrm{ss}}$, $\bar{c}_{iv}$ where ($i = A, B$). Also, $f_i(z)$ will not be a function of z, and will be replaced by f_i where ($i = 1, 2$).

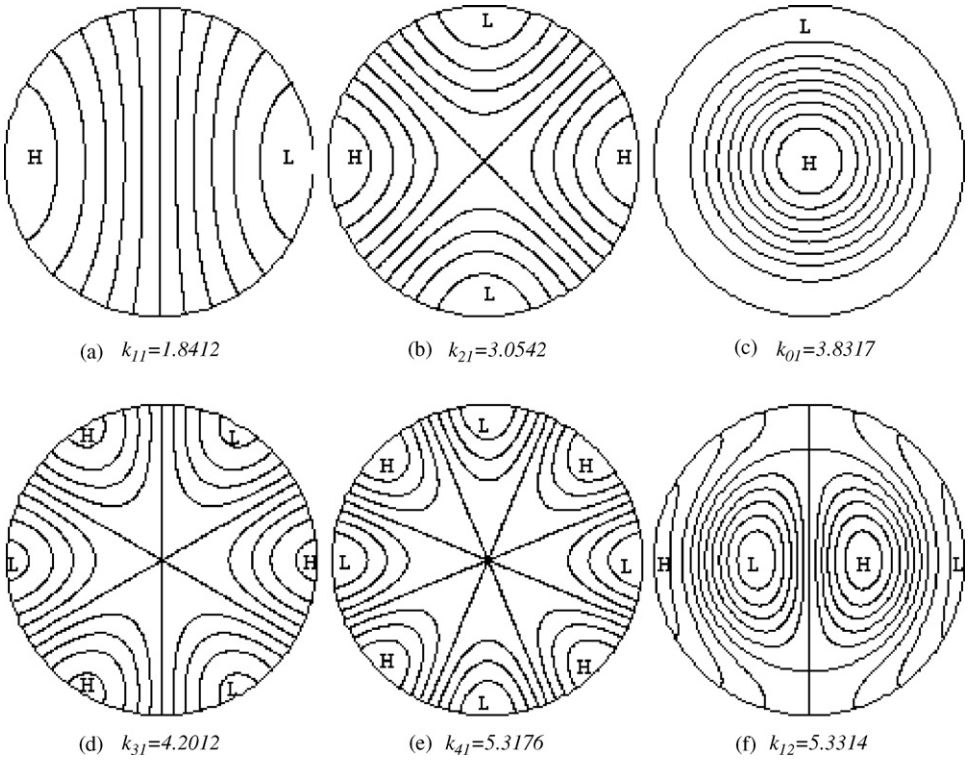

Fig. 2. The first six transverse eigen modes.

By linearizing the model equations using multivariate Taylor series expansion and substituting the perturbation terms (with $\lambda = 0$ for neutral stability analysis), we obtain the neutral stability relations for each of the three models, which are then solved to obtain the neutral stability boundary. Detailed derivation of the neutral stability relations for the 3D, averaged and regularized 2D models have been presented in Appendix A. Here we present the neutral stability relations for each of the three models.

Neutral stability relation for the three-dimensional model is a $(N-1)$th order polynomial in (k_{mn}^2/p) given by

$$\alpha_1\left(\frac{k_{mn}^2}{p}\right)^{N-1} + \alpha_2\left(\frac{k_{mn}^2}{p}\right)^{N-2} + \alpha_3\left(\frac{k_{mn}^2}{p}\right)^{N-3} + \cdots + \alpha_{N-1}\left(\frac{k_{mn}^2}{p}\right) + \alpha_N = 0, \tag{70}$$

where N is the total number of points in the second-order finite difference discretization scheme. The neutral stability relation obtained above can now be used to find the value of transverse Péclet number p for a given value of Da, β and μ. Neutral stability curves in the parameter space of p versus Da can also be plotted using this relation.

The neutral stability relations for the two low-dimensional models are quadratics equation in (k_{mn}^2/p), given by

$$\left(\frac{k_{mn}^2}{p}\right)^2 + [2\kappa + Da\,\bar{c}_{B,ss}(\bar{c}_{B,ss} - 2\bar{c}_{A,ss})]\left(\frac{k_{mn}^2}{p}\right) + [\kappa^2 + Da\,\bar{c}_{B,ss}(\bar{c}_{B,ss} - 2\bar{c}_{A,ss})\kappa] = 0, \tag{71}$$

where κ is given by

$$\kappa = \begin{cases} \left(1 - \dfrac{Da}{6\beta}\right)^{-1} & \text{for Averaged Model,} \\ \left(1 + \dfrac{Da}{6\beta}\right) & \text{for Regularized Model.} \end{cases} \tag{72}$$

Eqs. (70)–(72) could be used to generate the neutral stability curves for different values of μ, k_{mn}, and β.

5. Results

5.1. Steady state bifurcation diagrams: comparison between three-dimensional and spatially averaged models (averaged and regularized)

In this section, we present the steady state bifurcation diagrams obtained from both the three- and two-dimensional models for different values of μ ($=C_{B,in}/C_{A,in}$) and β ($=Da/Pe$). Solving the model equations given in Sections 3.1 and 3.2, we obtain bifurcation plots with steady state conversion of A (X_A) plotted against Damköhler number (Da). Fig. 3 presents two such bifurcation plots that show the effect of the parameter μ. Fig. 3(a) shows that for all the three models, the steady state bifurcation diagram is an S-shaped curve with three steady states over a range of Damköhler number, while Fig. 3(b) reveals that this region of steady state multiplicity decreases as μ increases, and at sufficiently high value of μ, the models have a single steady state solution over the complete range of Da. Larger the value of μ, higher is the concentration of species B in the inlet and larger is the autocatalytic effect, leading to very fast reaction and almost instantaneous consumption of species A, resulting in a single steady state rather than three. The reactor, therefore, jumps directly from the extinguished state to ignited one without going through that region in the param-

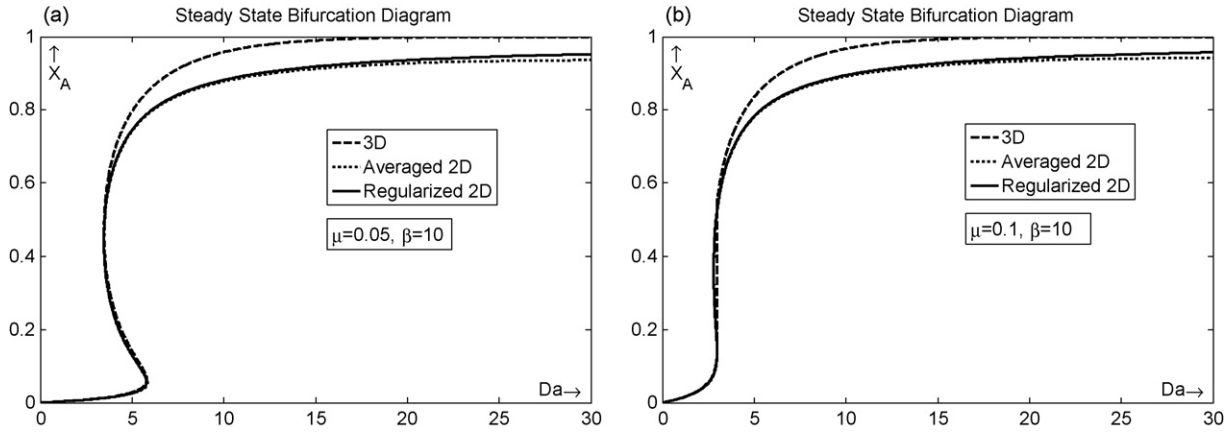

Fig. 3. Steady state bifurcation plots of exit conversion of A (X_A) versus Da, for all the three models, for (a) $\mu = 0.05$ and $\beta = 10$, (b) $\mu = 0.1$ and $\beta = 10$.

eter space where multiple steady states exist. As is evident from Fig. 3(a) and (b), the low-dimensional models retain this qualitative feature exhibited by the full 3D CDR model, and the bifurcation plots of the averaged and regularized models almost overlap each other for all values of μ. They diverge slightly from the bifurcation plots of three-dimensional model for large values of Da but are still quite accurate in predicting the region of steady state multiplicity for the complete range of μ. Large Da values imply longer reactors that make axial averaging less accurate. It has been shown for the case of catalytic reactors [18] that non-uniform pattern states emerge from the unstable middle branch of the bifurcation diagram. We shall illustrate with the help of linear stability computations that the same also holds true for the present case.

Fig. 4 shows similar bifurcation plots illustrating the effect of the parameter β. A comparison of the plots in Fig. 4(a)–(d) reveals that the region of multiplicity increases with a decrease in β. For a given value of Da, a decrease in β indicates an increase in Pe. Thus, an enlarged region of multiplicity corresponds to an increase in Pe or an increase in axial mixing limitations, which along with the transverse mixing limitations enhance the chances of pattern formation. A comparison of the curves for the three models shows that at higher values of β (between 10 and 20), the bifurcation diagrams of the two low-dimensional models coincide and are close to that

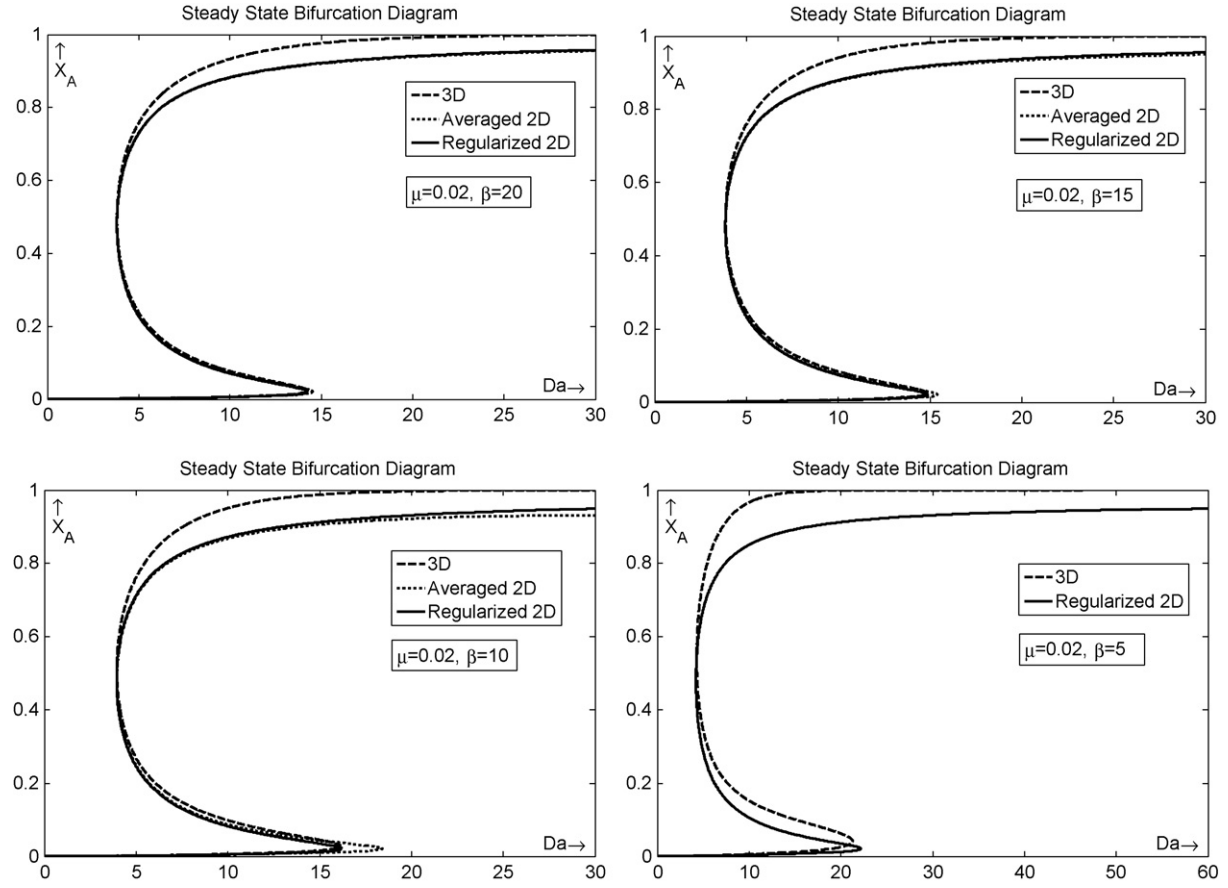

Fig. 4. Steady state bifurcation plots of exit conversion of A (X_A) versus Da, for all the three models, for four different values of β and $\mu = 0.02$.

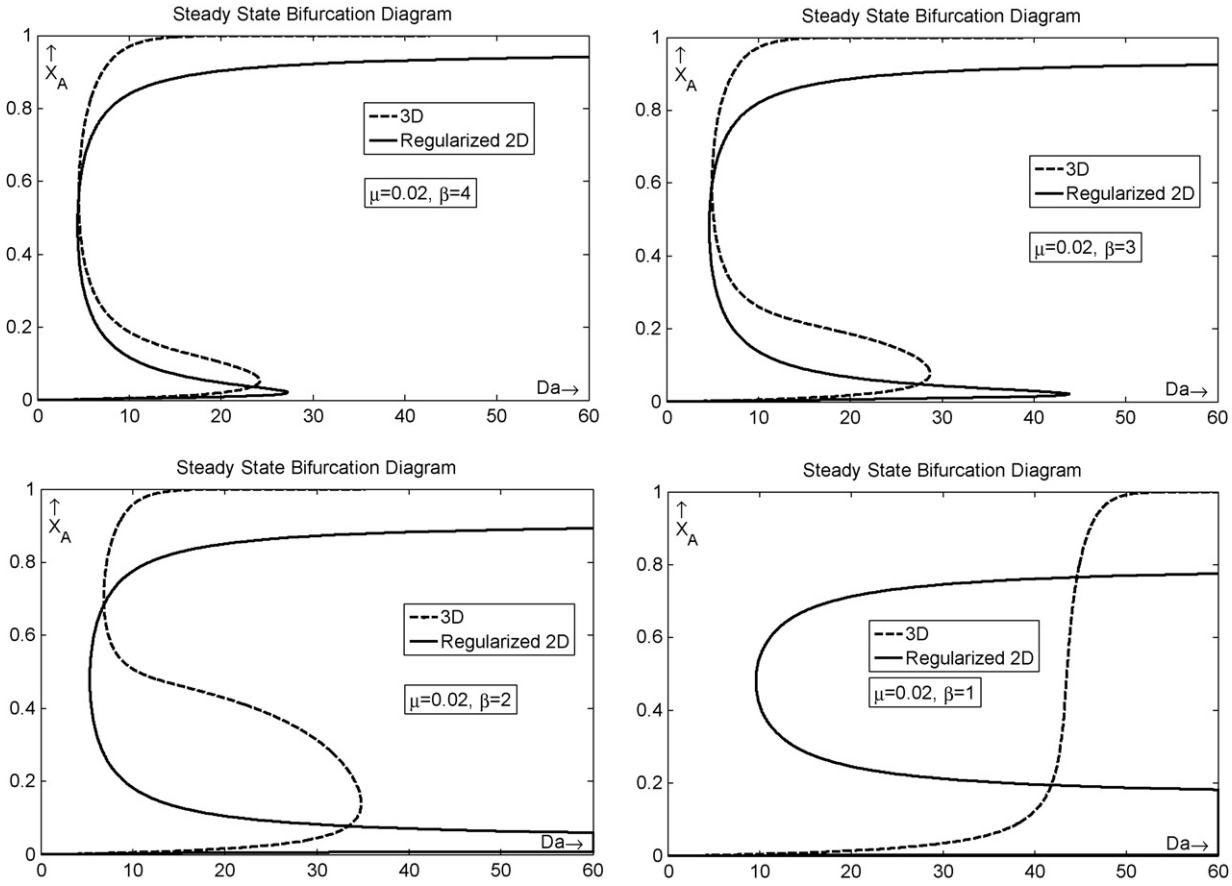

Fig. 5. Steady state bifurcation diagram plots for different values of β.

of the 3D model. Decreasing β causes the bifurcation plots of the low-dimensional models to diverge from those of the 3D model. It may be noted that decreasing β from 20 to 10 causes the averaged model to diverge more (especially near the point of extinction) than the regularized model, suggesting that the averaged model loses its accuracy at lower values of β (or at higher values of *Pe*) as we approach the border of convergence of the local equation. Fig. 4(d) shows bifurcation plots for the 3D and regularized models at $\beta = 5$. As is evident from the preceding discussion, the averaged model, which becomes increasingly inaccurate, does not yield an S-shaped bifurcation curve at values of $\beta \leq 9$. Therefore, for higher values of β, the averaged model is both quantitatively and qualitatively accurate, while at lower β values it loses quantitative agreement with the 3D model and ceases to be qualitatively valid for $\beta \leq 9$.

Fig. 5(a) and (b) shows the bifurcation plots for even lower values of $\beta = 4$ and $\beta = 3$, respectively. Even at $\beta = 4$ the regularized model shows reasonable agreement with the 3D model; however for $\beta = 3$ it starts to diverge and the divergence increases as β decreases. For $\beta \leq 2$ (when $\mu = 0.02$), the regularized model becomes both qualitatively and quantitatively inaccurate.

Thus, while the averaged model is valid for $\beta > 9$, the regularized model has a much larger region of validity given by $\beta > 2$.

5.2. Neutral stability curves: comparison between three-dimensional and spatially averaged models (averaged and regularized)

Using the neutral stability relations obtained in Section 4, we plot the neutral stability curves in the parameter space of transverse Péclet number, *p*, and Damköhler number, *Da*. Fig. 6(a)–(c) shows the neutral stability curves of all three models for the first four eigen modes, computed at $\beta = 10$ and $\mu = 0.02$, which – it turns out – are confined by two asymptotes. Fig. 6(d) compares the neutral stability curves of the three models for the third eigen mode k_{01}. In this case, complete agreement between the 3D and the regularized form of low dimensional model is observed.

Fig. 7 shows the effect of μ on the neutral stability curves. Inspection of Figs. 7 and 3(a) reveals that the two vertical asymptotes on either side of the neutral stability curve corresponds to the two limit points (i.e., the ignition and extinction points) in the corresponding steady state bifurcation diagram. Thus, the patterned states may emerge from the unstable middle branch that connects the two limit points of the bifurcation diagram. While Fig. 7(a) shows the regularized and the 3D models coinciding, Fig. 7(b) shows that no neutral stability curve is obtained for the three-dimensional model for $\mu \geq 0.1$ since there is no region of multiplicity for $\mu \geq 0.1$, which can also be seen from the corresponding bifurcation plot in Fig. 3(b). However, the two-dimensional models (both the averaged and the regularized) do predict a very small region of steady state multiplicity and hence we obtain neutral stability curves for them, as can be seen in Fig. 7(b). For still higher values of μ, the low-dimensional models follow the behavior of the 3D model in that no multiplicity is predicted by in any of the models.

Fig. 8 shows the effect of varying β from 20 to 5, corresponding to the parametric analyses of steady state bifurcation diagrams in Fig. 4. For $\beta \geq 10$, we observe the neutral stability curves of the regularized and the 3D models coincide completely while those of the averaged model diverge slightly from them. However, decreasing β causes the averaged model to diverge substantially from the

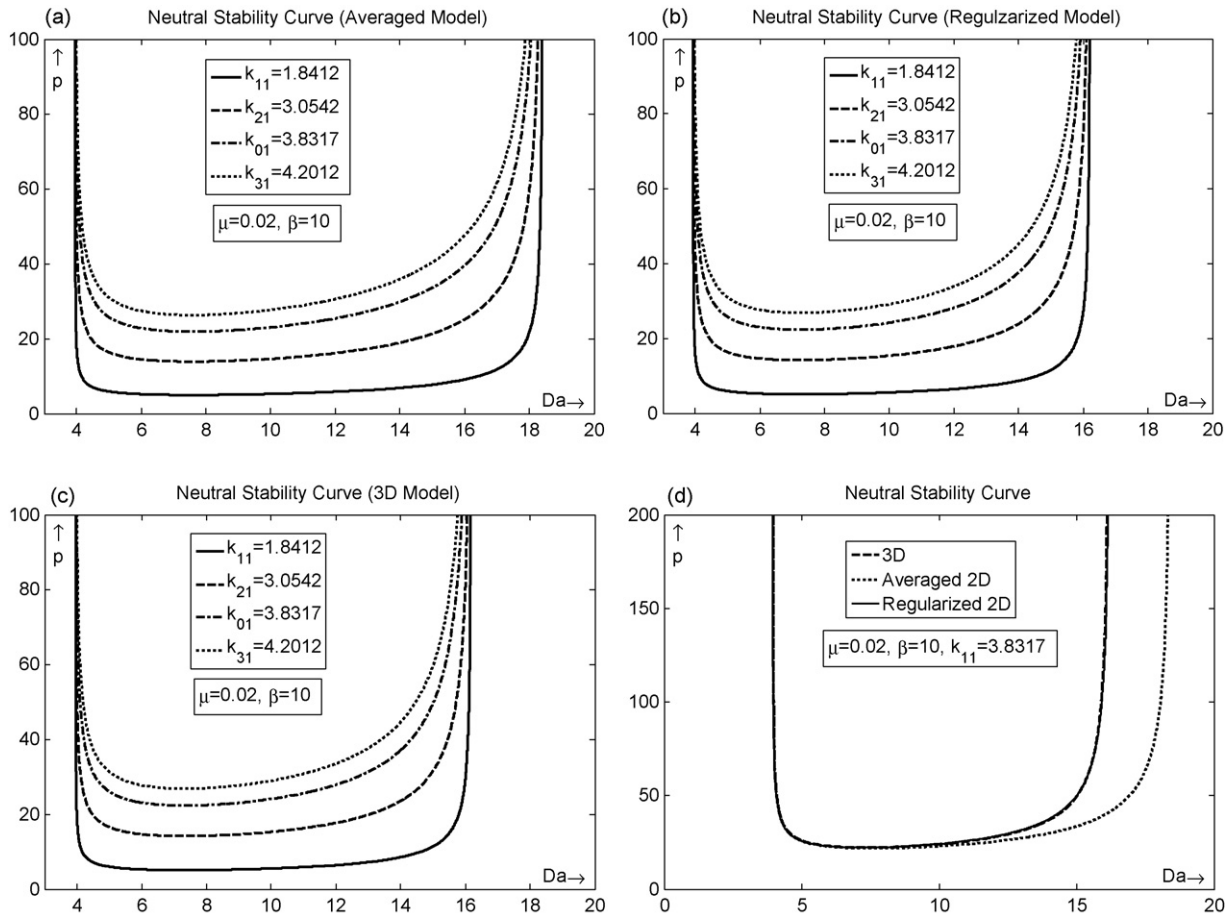

Fig. 6. Comparison of neutral stability curves for the three models. (a–c) Correspond to the first four eigen modes for the three models for the case of $\beta = 10$ and $\mu = 0.02$. (d) Compares the third mode of neutral stability curve of the three models for the case of $\beta = 10$ and $\mu = 0.02$.

three-dimensional model, as had been illustrated by the bifurcation diagrams.

6. Discussion and conclusions

In this work, we perform bifurcation and stability analysis of the three models of an isothermal homogeneous tubular reactor with autocatalytic kinetics. We start with the three-dimensional CDR equation, which is then averaged axially using Liapunov–Schmidt technique of classical bifurcation theory to obtain a two-dimensional model. *The region of validity of this averaged two-dimensional model is increased by regularizing it using the mathematical technique of regularization*. Steady state bifurcation diagrams that capture the steady state multiplicity of all three models are plotted and linear stability analysis is performed to determine the stability of these steady states to transverse

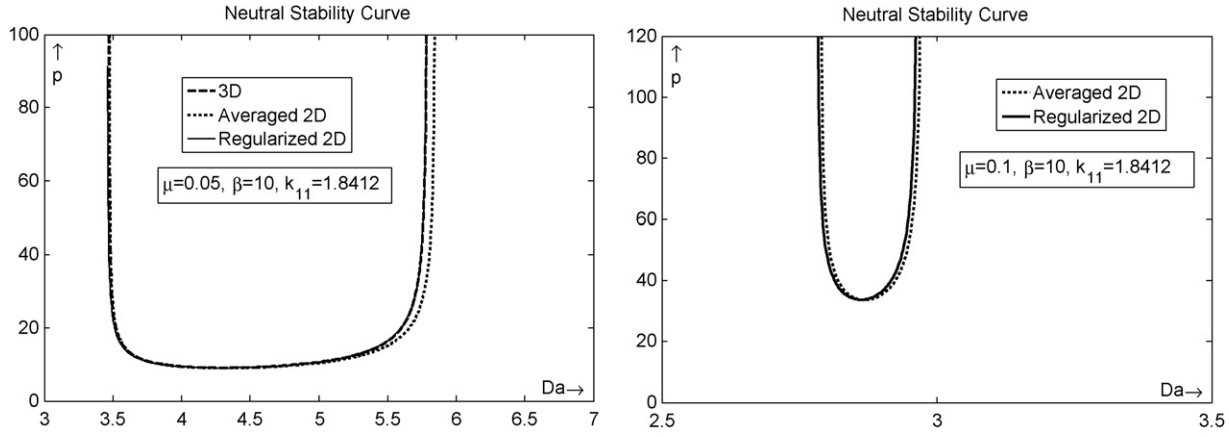

Fig. 7. Neutral stability curves for the three models corresponding to first eigen mode k_{11} for different values of μ and $\beta = 10$.

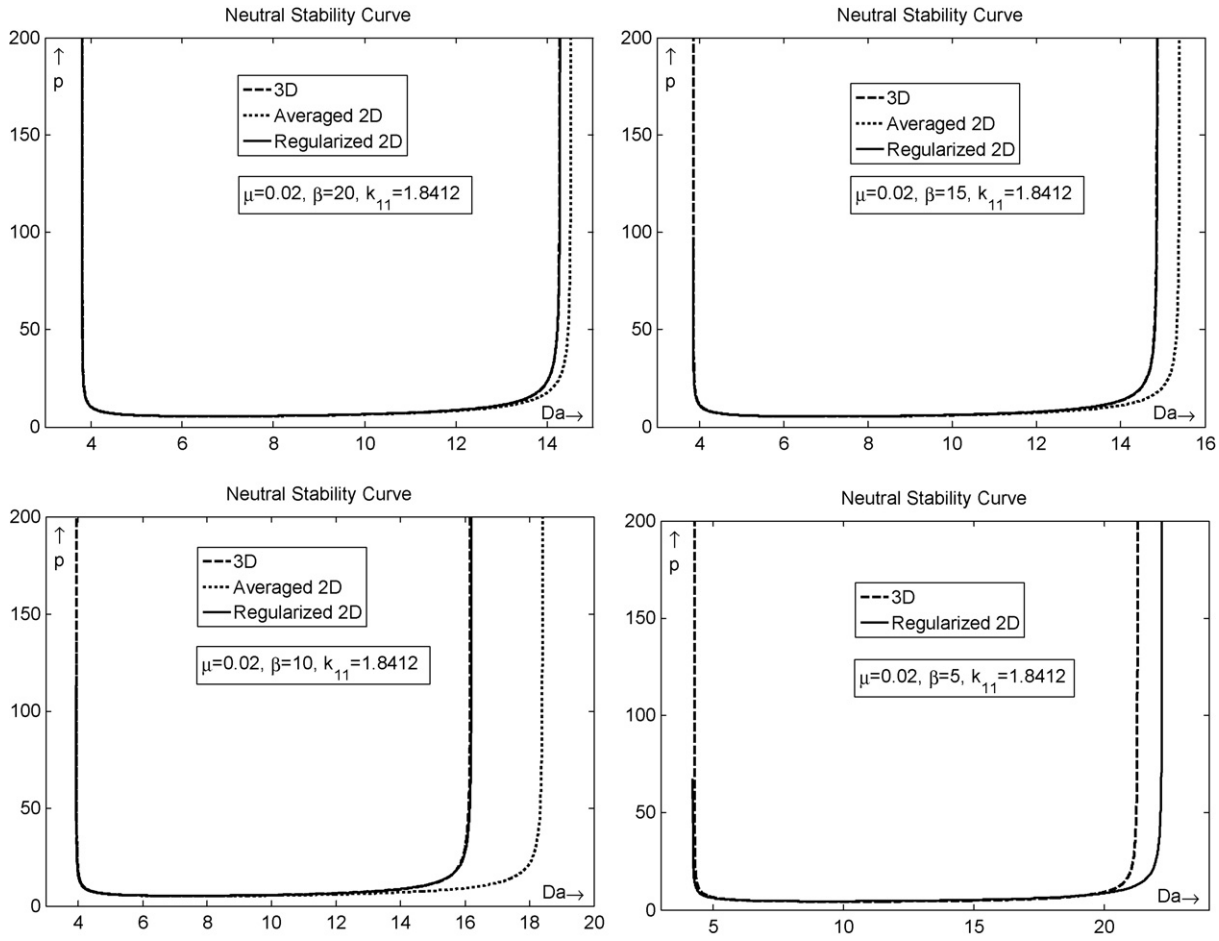

Fig. 8. Comparison of neutral stability curves using the three models corresponding to first eigen mode k_{11} for different values of β and $\mu = 0.02$.

perturbations. *Analytical expressions of steady states and stability boundaries obtained for the low-dimensional case provide considerable computational ease over those given by the second order partial differential equations for 3D model.* Our results show that for all the three models, the two asymptotes of the neutral stability curve correspond to the two limit points (ignition and extinction points) of the bifurcation diagram. Thus, we may conclude that for the case of homogeneous autocatalysis patterned states may emanate from the unstable middle branch connecting the ignition and extinction points in the S-shaped bifurcation curve as in the case of catalytic reactors [18]. Our neutral stability results indicate that the patterned states may be observed more readily for low values of μ (inlet feeding ratio of B to A).

Comparison of bifurcation diagrams and neutral stability curves of the three models indicates that while the averaged model is quantitatively correct for $\beta > 9$, the regularized model is both qualitatively and quantitatively accurate for $\beta \geq 5$ and is qualitatively correct up to $\beta > 2$. Thus, while the regularized model is valid for $\beta > 2$, the averaged model is valid for $\beta > 9$, and the former is therefore recommended over the latter.

A computational analysis of the temporal evolution of mixing-limited concentration and temperature patterns has been performed using averaged and regularized models for the isothermal [29] and non-isothermal [30] cases. Our analysis shows that the patterned states indeed emerge from the middle unstable branch of the S-shaped bifurcation curve, and the temporal evolution of patterned states is characterized by a process of concentration-segregation followed by a gradual decay of non-homogeneity, which eventually results in a homogeneous stable steady state. The above-referred works also confirm that the time required for the patterned states to decay into homogeneous states is strongly dependent on the transverse and axial Péclet numbers. As may be intuitively expected, an increase in the values of these numbers results in an increased decay time of patterned states.

Appendix A. Calculation of linear stability boundary

In this section, we present the derivation of the neutral stability relations for the three models.

A.1. Calculation of neutral stability boundary for three-dimensional model

Using Eqs. (15), (67), (68) we linearize non-linear reaction terms using multivariate Taylor series expansion truncated at first-order to get

$$\begin{aligned} \lambda f_1 + f_1' &= \frac{\beta}{Da} f_1'' - \frac{k_{mn}^2}{p} f_1 - Da(C_{B,ss}^2 f_1 + 2C_{A,ss} C_{B,ss} f_2), \\ \lambda f_2 + f_2' &= \frac{\beta}{Da} f_2'' - \frac{k_{mn}^2}{p} f_2 + Da(C_{B,ss}^2 f_1 + 2C_{A,ss} C_{B,ss} f_2), \end{aligned} \tag{73}$$

with the boundary conditions

$$\begin{aligned} \text{At } z = 0, \quad & \frac{\beta}{Da} f_1' = f_1, \\ & \frac{\beta}{Da} f_2' = f_2. \end{aligned} \tag{74}$$

$$\begin{aligned} &\text{At } z = 1, \quad f_1' = 0, \\ &\qquad\quad f_2' = 0. \end{aligned} \tag{75}$$

In order to obtain the neutral stability relations, we substitute $\lambda = 0$ in Eq. (73). Adding the equations for species A and B in Eqs. (73)–(75) and solving for $(f_1 + f_2)$, we get

$$f_1 + f_2 = 0. \tag{76}$$

Substituting Eq. (76) in Eq. (73), and keeping $\lambda = 0$, we get

$$\begin{aligned} &\frac{\mathrm{d}f_1}{\mathrm{d}z} = \frac{\beta}{Da}\frac{\mathrm{d}^2 f_1}{\mathrm{d}z^2} - \frac{k_{mn}^2}{p} f_1 - Da(C_{B,ss}^2 f_1 - 2C_{A,ss}C_{B,ss}f_1), \\ &\text{At } z = 0, \quad \frac{\beta}{Da} f_1' = f_1, \\ &\text{At } z = 1, \quad f_1' = 0. \end{aligned} \tag{77}$$

Similar to the steady state solution of the three-dimensional model, we discretize the second-order ordinary differential equation by using second order central difference scheme with reflection boundary conditions. We discretize the domain $z = 0$ to $z = 1$ using $N - 1$ points, which results in the following system of homogeneous linear equations with $(N + 1)$ equations and $(N + 1)$ variables

$$Af = B, \tag{78}$$

where

$$A = \begin{bmatrix} a_{11} & a_{12} & a_{13} & 0 & 0 & \cdots & 0 \\ a_{21} & a_{22} & a_{23} & 0 & 0 & \cdots & 0 \\ 0 & a_{32} & a_{33} & a_{34} & 0 & \cdots & 0 \\ 0 & 0 & \ddots & \ddots & \ddots & 0 & 0 \\ 0 & \cdots & 0 & a_{N-1,N-2} & a_{N-1,N-1} & a_{N-1,N} & 0 \\ 0 & \cdots & 0 & 0 & a_{N,N-1} & a_{N,N} & a_{N,N+1} \\ 0 & \cdots & 0 & 0 & a_{N+1,N-1} & a_{N+1,N} & a_{N+1,N+1} \end{bmatrix}, \tag{79}$$

$$\begin{aligned} &f = [f_{1,1} f_{1,2} f_{1,3} \ldots f_{1,N+1}]^{\mathrm{T}}, \\ &B = [0\,0\,0 \ldots 0]^{\mathrm{T}}. \end{aligned} \tag{80}$$

Patterned states will exist in the reactor only if the above system of equations has a non-trivial solution, i.e., when

$$\det(A) = 0. \tag{81}$$

Using Eq. (81), we obtain a neutral stability relation of the form

$$\alpha_1 \left(\frac{k_{mn}^2}{p}\right)^{N-1} + \alpha_2 \left(\frac{k_{mn}^2}{p}\right)^{N-2} + \alpha_3 \left(\frac{k_{mn}^2}{p}\right)^{N-3} + \cdots + \alpha_{N-1} \left(\frac{k_{mn}^2}{p}\right) + \alpha_N = 0. \tag{82}$$

The values of parameters $\alpha_1, \alpha_2, \ldots, \alpha_N$ depend on Da, the steady state concentrations of both species, β, k_{mn} and N.

A.2. Calculation of neutral stability boundary for the averaged model

Using Eqs. (47), (67), (68) we linearize the non-linear reaction terms using multivariate Taylor series expansion truncated at first order to get

$$\begin{aligned} p\left[\lambda f_1 + \frac{1}{1 - (Da/6\beta)} f_1 + Da(\bar{c}_{B,ss}^2 f_1 + 2\bar{c}_{A,ss}\bar{c}_{B,ss} f_2)\right] &= -k_{mn}^2 f_1 \\ p\left[\lambda f_2 + \frac{1}{1 - (Da/6\beta)} f_2 - Da(\bar{c}_{B,ss}^2 f_1 + 2\bar{c}_{A,ss}\bar{c}_{B,ss} f_2)\right] &= -k_{mn}^2 f_2. \end{aligned} \tag{83}$$

We substitute $\lambda = 0$ for neutral stability analysis. Writing the above equations in matrix notation, we get

$$\begin{bmatrix} \frac{1}{1 - (Da/6\beta)} + Da\ \bar{c}_{B,ss}^2 + \frac{k_{mn}^2}{p} & 2Da\,\bar{c}_{A,ss}\bar{c}_{B,ss} \\ -Da\,\bar{c}_{B,ss}^2 & \frac{1}{1 - (Da/6\beta)} - 2Da\ \bar{c}_{A,ss}\bar{c}_{B,ss} + \frac{k_{mn}^2}{p} \end{bmatrix} \begin{bmatrix} f_1 \\ f_2 \end{bmatrix} = 0. \tag{84}$$

Similar to the three-dimensional case, for patterned states to exist, the above system of homogeneous linear equations should admit a non-trivial solution, which occurs when

$$\begin{vmatrix} \frac{1}{1 - (Da/6\beta)} + Da\ \bar{c}_{B,ss}^2 + \frac{k_{mn}^2}{p} & 2Da\,\bar{c}_{A,ss}\bar{c}_{B,ss} \\ -Da\,\bar{c}_{B,ss}^2 & \frac{1}{1 - (Da/6\beta)} - 2Da\ \bar{c}_{A,ss}\bar{c}_{B,ss} + \frac{k_{mn}^2}{p} \end{vmatrix} = 0. \tag{85}$$

Using Eq. (85), we obtain the neutral stability relation,

$$\left(\frac{k_{mn}^2}{p}\right)^2 + \left[\frac{2}{(1 - (Da/6\beta))} + Da\ \bar{c}_{B,ss}(\bar{c}_{B,ss} - 2\bar{c}_{A,ss})\right]\left(\frac{k_{mn}^2}{p}\right) \times \left[\frac{1}{(1 - (Da/6\beta))^2} + Da\ \bar{c}_{B,ss}(\bar{c}_{B,ss} - 2\bar{c}_{A,ss})\frac{1}{(1 - (Da/6\beta))}\right] = 0. \tag{86}$$

A.3. Calculation of neutral stability boundary for the regularized model

Following the same procedure as in the case of averaged model, we obtain a neutral stability relation (similar to Eq. (86)) for the regularized model as

$$\left(\frac{k_{mn}^2}{p}\right)^2 + \left[2\left(1 + \frac{Da}{6\beta}\right) + Da\ \bar{c}_{B,ss}(\bar{c}_{B,ss} - 2\bar{c}_{A,ss})\right]\left(\frac{k_{mn}^2}{p}\right) \left[\left(1 + \frac{Da}{6\beta}\right)^2 + Da\ \bar{c}_{B,ss}(\bar{c}_{B,ss} - 2\bar{c}_{A,ss})\left(1 + \frac{Da}{6\beta}\right)\right] = 0. \tag{87}$$

The neutral stability curves can be plotted in the parameter space of p versus Da by using the above neutral stability relations.

References

[1] A.M. Turing, The chemical basis for morphogenesis, Phil. Trans. Royal Soc. Lond. B: Biol. Sci. 237 (1952) 37–72.
[2] G. Nicolis, I. Prigogine, Symmetry breaking and pattern selection in far-from-equilibrium systems, Proc. Natl. Acad. Sci. U.S.A. 78 (1981) 659.
[3] G. Nicolis, I. Prigogine, Self-organisation in Non-equilibrium Chemical Systems, Wiley, New York, 1977.
[4] I. Prigogine, R. Lefever, On symmetry-breaking instabilities in dissipative systems, J. Chem. Phys. 46 (1967) 3542.
[5] I. Prigogine, R. Lefever, Symmetry breaking instabilities in dissipative systems II, J. Chem. Phys. 48 (1968) 1695.
[6] G.K. Boreskov, YuSh Matros, O.P. Klenov, V.I. Logovkoi, V.S. Lakhmostov, Local nonuniformities in a catalyst bed, Dokl. Akad. Nauk. S.S.S.R. 258 (1981) 1418–1420.
[7] Y.S. Matros, Unsteady Processes in Catalytic Reactors, Elsevier, Amsterdam, 1985.
[8] C.H. Barkelew, B.S. Gambhir, Stability of trickle-bed reactors, ACS Sym. Series 237 (1984) 61–81.
[9] B. Marwaha, D. Luss, Formation and dynamics of a hot zone in radial flow reactor, AIChE J. 48 (2002) 617–624.
[10] B. Marwaha, S. Sundarram, D. Luss, Dynamics of transversal hot zones in shallow packed bed reactors, J. Phys. Chem. B 108 (2004) 14470–14476.
[11] D. Luss, J.E. Bailey, S. Sharma, Asymmetric steady-states in catalytic slabs with uniform and nonuniform environments, Chem. Eng. Sci. 27 (1972) 1555.
[12] R.A. Schmitz, T.T. Tsotsis, Spatially patterned states in systems of interacting catalyst particles, Chem. Eng. Sci. 38 (1983) 1431–1437.
[13] F. Stroh, V. Balakotaiah, Modeling of reaction induced flow maldistributions in packed-beds, AIChE J. 37 (1991) 1035–1052.

[14] D. Nguyen, V. Balakotaiah, Flow maldistributions and hot spots in down-flow packed bed reactors, Chem. Eng. Sci. 49 (1994) 5489–5505.
[15] D. Nguyen, V. Balakotaiah, Reaction-driven instabilities in down-flow packed beds, Proc. Math. Phys. Sci. 450 (1995) 1–21.
[16] A.H. Benneker, A.E. Kronberg, K.R. Westerterp, Influence of buoyancy forces on the flow of gases through packed beds at elevated pressures, AIChE J. 44 (1998) 263–270.
[17] V. Balakotaiah, E.L. Christaforatou, D.H. West, Transverse concentration and temperature non-uniformities in adiabatic packed bed catalytic reactors, Chem. Eng. Sci. 54 (1999) 725–1734.
[18] V. Balakotaiah, N. Gupta, D.H. West, Transport limited pattern formation in catalytic monoliths, Chem. Eng. Sci. 57 (2002) 435–448.
[19] M. Sheintuch, O. Nekhamkina, Pattern formation in homogeneous reactor models, AIChE J. 45 (1998) 398–409.
[20] G.A. Viswanathan, D. Luss, Model prediction of hot spots. Formation in shallow adiabatic packed-bed reactors, AIChE J. 52 (2006) 1533–1538.
[21] G.A. Viswanathan, D. Luss, Hot zones formation and dynamics in long adiabatic packed-bed reactors, Ind. Eng. Chem. Res. 45 (2006) 7057–7066.
[22] G.A. Viswanathan, D. Luss, Moving transversal hot zones in adiabatic, shallow packed-bed reactors, AIChE J. 52 (2006) 705–717.
[23] S. Chakraborty, V. Balakotaiah, Low-dimensional models for describing mixing effects in laminar flow tubular reactors, Chem. Eng. Sci. 57 (2002) 2545.
[24] S. Chakraborty, V. Balakotaiah, Two-mode models for describing mixing effects in homogeneous reactors, AIChE J. 48 (2002) 2571–2586.
[25] S. Chakraborty, V. Balakotaiah, Multi-mode low-dimensional models for non-isothermal homogeneous and catalytic reactors, Chem. Eng. Sci. 59 (2004) 3695–3724.
[26] S. Chakraborty, V. Balakotaiah, Spatially averaged multi-scale models for chemical reactors, in: B. Marin Guy (Ed.), Advances in Chemical Engineering, 30, Academic Press, 2005, pp. 205–297.
[27] M. Golubitsky, D.G. Schaeffer, Singularities and Groups in Bifurcation Theory, vol. 1, Springer-Verlag, New York, 1985.
[28] S. Chakraborty, averaging theory and low-dimensional models for homogeneous and catalytic reactors. Ph.D. Dissertation (2003), University of Houston.
[29] A. Gupta, S. Chakraborty, Dynamic simulation of mixing-limited pattern formation in homogeneous autocatalytic reactions, Chem. Prod. Process Model. 3 (2) (2008), Article 9.
[30] S. Chakraborty, A. Gupta, Temporal evolution of mixing-limited spatial patterns in non-isothermal homogeneous reactors, J. Chem. Eng. Jpn. (2008), in review.
[31] O. Takeshi, Surface equation of falling film flows with moderate Reynolds number and large but finite Weber number, Phys. Fluids 11 (1999) 3247–3269.